LEGIBILITY NOTICE

A major purpose of the Technical Information Center is to provide the broadest dissemination possible of information contained in DOE's Research and Development Reports to business, industry, the academic community, and federal, state and local governments.

Although a small portion of this report is not reproducible, it is being made available to expedite the availability of information on the research discussed herein.

LA-UR-88-1265

LA-UR--88-1265

DE88 009127

TITLE ANALYSES OF SWEEP-UP, EJECTA, AND FALLBACK MATERIAL FROM THE 4250 METRIC TON HIGH EXPLOSIVE TEST "MISTY PICTURE"

AUTHOR(S) Kenneth H. Wohletz, Robert Raymond, Jr., Glen Rawson,[1] and Tom Mazzola[1]

SUBMITTED TO Smoke/Obscurants Symposium XII
Kossiakoff Conference and Education Center
The Johns Hopkins University
Laurel, MD 20707
April 19-21, 1988

[1]R&D Associates, Marina del Rey, CA 90295

Los Alamos Los Alamos National Laboratory
Los Alamos, New Mexico 87545

FORM NO. 836 R4
ST. NO. 2629 5/81

ANALYSES OF SWEEP-UP, EJECTA, AND FALLBACK MATERIAL FROM THE 4250 METRIC TON HIGH EXPLOSIVE TEST "MISTY PICTURE"

Kenneth H. Wohletz and Robert Raymond, Jr.
Los Alamos National Laboratory
Los Alamos, New Mexico, 87545

Glen Rawson (consultant) and Tom Mazzola
R&D Associates, Marina del Rey, California, 90295

ABSTRACT

The MISTY PICTURE surface burst was detonated at the White Sands Missle Range in May of 1987. The Los Alamos National Laboratory dust characterization program was exparded to help correlate and interrelate aspects of the overall MISTY PICTURE dust and ejecta characterization program. Pre-shot sampling of the test bed included composite samples from 15 to 75 m distance from Surface Ground Zero (SGZ) representing depths down to 2.5 m, interval samples from 15 to 25 m from SGZ representing depths down to 3 m, and samples of surface material (top 0.5 cm) out to distances of 190 m from SGZ. Ejecta and fallout samples were collected mostly along 3 radials (225, 270, and 337) from the crater lip to distances of 900 m from SGZ. Sweep-up samples were collected in GREG/SNOB gages located within the DPR. All samples were dry-sieved between 8.0 mm and 0.045 mm (16 size fractions); selected samples were analyzed for fines by a centrifugal settling technique. The size distributions were analyzed using spectral decomposition based upon a sequential fragmentation model. Results suggest that the same particle size subpopulations are present in the ejecta, fallout, and sweep-up samples as are present in the pre-shot test bed. The particle size distribution in post-shot environments apparently can be modelled taking into account heterogeneities in the pre-shot test bed and dominant wind direction during and following the shot.

I. INTRODUCTION

The MISTY PICTURE surface burst of 4250 metric tons of ammonium nitrate and fuel oil (ANFO) was detonated at the White Sands Missile Range (WSMR) in May of 1987. The primary purpose of the test was to simulate the air blast environment of a low kiloton yield nuclear explosion. A similar test of 4017 metric tons, code name MINOR SCALE, was conducted there in 1985 very close to the MISTY PICTURE site. The Los Alamos National Laboratory (LANL) dust characterization program was initiated on MINOR SCALE and greatly expanded for MISTY PICTURE. The results described in

this report are for a dust and ejecta sampling and analysis effort, initiated to help correlate and interrelate aspects of the overall dust and ejecta characterization program. A unique aspect of this work is the examination of sweep-up samples collected from sites subjected to peak air blast pressures ranging from 1.7×10^5Pa to 5.44×10^5Pa. Sampling heights ranged from 2.5 cm to 150 cm above the ground. These sweep-up data are compared with analyses of samples from the explosion test bed, fallout and ejecta samples, and fallback material located very near the crater, and with analyses of reconstituted soil make by B. Phillips (1987). Particle size data for the different environments are decomposed into sub-populations that reflect size of starting materials and can be used to infer the mechanisms of fragmentation and transport for different size ranges.

2. BACKGROUND

Dust characterization of simulated nuclear explosions is an evolving discipline. One reason for presenting this report is to ensure that sampling and analyses can be better coordinated and planned for in the future. LANL and R & D Associates (RDA) first jointly studied dust as part of the Defense Nuclear Agency's (DNA) field programs on MINOR SCALE. During MINOR SCALE two chemical tracers were placed separately in the explosive and on the ground surrounding the charge to help track the mass of dust lofted to the stablized cloud. The experiment was envisioned as a mechanism to investigate the value of the tracer emplacement technique. By using aircraft-mounted sampling filters in pods, the dust cloud resulting from the detonation was sampled from its top at 4.6 km to its base at 1.7 km with 10 sampling traverses. Results of the MINOR SCALE tracer experiment can be found in Mason et al. (1987). Results of that study

showed that the total dust lofted was $3x10^9$ grams. The cloud was distinctly bimodal with dust maxima at 4.1 km and 2.9 km. The upper mass peak was enriched in the explosive tracer and represented the more buoyant fireball fraction of the cloud. The lower altitude peak was enriched in the soil tracer emplaced around the charge.

The tracer approach was expanded for MISTY PICTURE. Three tracers were emplaced in the charge and 8 tracers were distributed along 8 radials at 45 degree intervals and at depths down to 1.8 m in material to be ejected in the cratering process. In addition 5 organic tracers were distributed along 8 radials at 45 degree intervals at ranges of 91.4 m to 915 m to tag sweep-up material. No tracers were added to the radial used to simulate the thermal layer of non-ideal dusty air blast where the reconstituted soil test bed had been prepared. LANL then fielded cloud and fallout sampling programs to characterize both general dust and tracer occurrence. Preliminary results have been reported separately (Bayhurst et al., 1988). The MISTY PICTURE event was detonated under a substantial cloud cover which made dust cloud detection and sampling more difficult than for MINOR SCALE. Furthermore, the time of cloud entry was delayed relative to that of MINOR SCALE. Both of these factors suggest that less than optimum samples may have been collected representing only part of the dust cloud. Estimates from weighed dust on the filters and computations based on tracer data were found to be $1x10^9$ gm, or 1/3 that of MINOR SCALE. However, this apparent mass lofted within the stablized cloud is most probably a minimal value.

Other agencies are making significant contributions to the MISTY PICTURE dust characterization program. Cloud and fallout samples were collected and are being studied by Science Applications Int. Corp. (SAIC) and Particle Measuring Systems Inc. (PMS). SAIC also has programs studying

the scouring of pebbles in the sweep-up region as well as tracking ejecta balls marked by flares in flight (Cockayne, personal communication; Wisotski, 1987). The Waterways Experiment Station of the Army (WES) has characterized the soil along the Dusty Precursed Radial (Phillips, 198 WES has also conducted an ejecta missile survey after the shot (Scott, in progress). New Mexico Engineering Research Institute (NMERI) has measured and documented crater size and shape, surface displacements, and the ejecta blanket extent and thickness (Benson, et al., 1988). Numerous marked ejecta objects from penny- to bowling-ball-size were also recovered. The US Geological Survey has photodocumented the crater and lip excavations and provided geotechnical interpretation (Benson et al., 1988).

As a supplement to the above projects, we were able to sample the MISTY PICTURE test bed prior to the shot and to collect sweep-up, ejecta, and fall-back material following the shot. In this paper we present details concerning the sampled materials that should have significant bearing on all interpretations of transport mechanisms resulting from the shot.

3. SAMPLING

All samples collected by LANL were double wrapped in sealed plastic bags. Since sample size prohibited statistically valid data for cobble and boulder sized particles, no particles larger than about 7.5 cm were collected. The largest boulders observed in the pretest trenches were about 45 cm x 60 cm in size. These large rocks occurred infrequently; 10 cm to 15 cm cobbles cropped out much more commonly along trench walls. GRIG/SNOB gage samples, collected by Aberdeen Research and H-Tech Laboratories, Inc., were sealed in small zip-lock plastic bags.

3.1 PRE-SHOT S .MPLING OF THE TEST BED

WES contracted to characterize soil of the Dusty Precursed Radial (DPR), an area that was later to be covered by helium-filled bags (discussed below). As part of this characterization, approximately the top 0.6 cm at 24 localities were sampled within the DPR. Average wet density and thickness measurements were made prior to the final loosening of the soil surface (Phillips, 1987).

Other than the sampling WES contracted for, no additional sampling was planned for the pre-shot test bed. However, considering the need for a comprehensive understanding of the starting materials, we collected samples at the test bed as opportunities became available. Augered drill holes for the LANL tracers and for the NMERI crater edge characterization using buried columns of colored sand provided an opportunity to sample intervals from the surface down to depths of 3 m. These are shown as open circles on figure 1 (labeled MULTIPLE HORIZONS SAMPLED). Composite samples from the surface down to depths of 2.5 m are shown as solid dots and were obtained from augered drill holes and electrical cable trenches. Near the zero azimuth radial, 4 samples of surface material (less than 1 cm depth) were collected, 2 at 160 m and 2 at 170 m to 190 m. Three of the samples are typical of the bladed test bed; the most distant sample was virgin soil composed of windblown silt.

3.2 POST-SHOT SAMPLING OF CLOSE-IN FALLOUT, EJECTA, AND FALLBACK MATERIAL

Fallout and ejecta sampling was restricted to concrete surfaces where it was unnecessary to define the boundary between deposited materials and the in situ soil surface. Dependent upon sample thickness, areas from 0.1 to 1.0 m^2 were sampled such that 1-2 kg samples were collected; mass per unit area could then readily be determined. Figure 2 shows the sampling locations of close-in ejecta and fallout. Dominant wind

direction during and following the MISTY PICTURE shot had a west north west trend. Thus radial 270 was closest to down wind and radials 225 and 337 were each approximately 50° off the dominant wind direction. Figure 3 provides the mass/area plots with respect to distance from SGZ for ejecta collected along radials 225, 270, and 337.

NMERI trench excavations of the crater lip revealed horizons that included fallback from the collapsed stem of the cloud. The upper two horizons were sampled at distances of 60 m and 67 m from SGZ (Figure 4).

3.3 SWEEP-UP SAMPLES FROM THE DUSTY PRECURSED RADIAL

The DPR contained a large area of reconstituted soil over which helium was emplaced beneath large plastic bags. This produced a low density "air" layer immediately above the ground that simulated the layer heated by thermal radiation from a nuclear burst. Within this layer were a number of GREG and SNOB gages to document the dusty flow and pressure history. The gage pairs differentiate gas pressure from the pressure exerted by the gas and dust mixture. The design of the SNOB gage includes a tube that is 3.8 mm in diameter. It is in these tubes that dust collects. In the absence of larger dust collectors, these provided swept-up samples of the prepared test bed. Because of the small quantities collected, individual samples were composited to enable analyses comparable to the other samples being studied. Compositing was based on pre-screening and microscopic examination (Rawson, 1987a,b).

Three sets of samples were collected from tubes where the GREG/SNOB gages were installed. LANL has obtained those supplied by Aberdeen Research Center from the Hard Mobile Launcher (HML) models at peak pressures of 2.0×10^5 Pa to 3.4×10^5 Pa, respectively at 278 m and 346 m.[1]

[1]Noel Ethridge of Aberdeen Research Center provided samples and locations.

The tubes were installed at heights ranging from 3.3 cm to 24 cm normal to both the front and rear inclined surfaces. Initial analyses of the small amounts of material in the 52 tubes indicated no systematic variations of particle size distribution or mass with either elevation or pressure (Rawson, 1987a). Thus it was determined all of these could be composited for analysis. The second set of samples were obtained from H-Tech.[2] These covered a pressure range from 1.7×10^5 Pa to 5.4×10^5 Pa and heights from 2.5 cm to 150 cm. The tubes were mounted parallel to the ground on vertical rakes. Preliminary analysis indicated variations mostly with elevation (Rawson, 1987b), so samples collected at heights from 2.5 cm to 23 cm were composited and those of heights 30 cm to 150 cm were composited. The size of the basal composite was chosen to to be comparable in height to that of the HML sample. Due to the small size of samples, the second composite had to include all remaining samples up to a height of 150 cm. A small number of samples held by Carpender Research Corporation have not been analyzed.

4. RESULTS

All samples were dry-sieved between 8.0 and 0.045 mm [-3ϕ to 4.5ϕ; $\phi = -\log_2$ (diameter in mm)], and selected samples were subjected to a fires analysis by a centrifugal settling technique between the sizes of 0.0625 and 0.0001 mm. The results of these size determinations were subjected to distribution analysis using a spectral decomposition (Sheridan et al., 1986) based upon the sequential fragmentation/transport (SFT) model of Wohletz et al. (1987; in press). The underlying assumption of this analysis is that sample particle-size distributions are composed of several

2Bruce Hartenbaum supplied samples and location information after samples had been collected, weighed, and examined.

subpopulations, as shown by the polymodal nature of their size-frequency histograms. A second assumption of the analysis is that the constituent subpopulations are not lognormally distributed in size, but are better-characterized by the SFT distribution.

The SFT distribution was first introduced by Brown (1986) as the sequential fragmentation distribution, which belongs to the Weibull family of distributions. Brown (in press) later showed that this model fits observed size distributions of many types of particular matter, including high explosive aerosols, ball mill products, and volcanic ash. Wohletz et al. (1987; in press) developed the SFT for application to geologic materials and advocate its application because it is a non-empirical distribution (contrasted with commonly used lognormal, Weibull, and Rossin-Rammler distributions). The SFT distribution is formulated to express the distribution of particle sizes derived from a sequence of fragmentation and transport processes by which an initial mass is broken step-wise into smaller fragments and sorted by one or more transporting processes. The form of the distribution is similar to that of the lognormal except that it has a built-in skewness, which is controlled by a free parameter γ:

$$\frac{dM}{d\phi} = K_2 L^G \exp\left[-\frac{L^{3(\gamma+1)}}{\gamma+1}\right] ,$$

where M is the sample mass retained in logarithmically spaced size bins (ϕ defined above), K_2 is unity for distribution totalling 100 %, L is particle diameter, and γ is the free parameter that determines the position and width of the distribution. This equation is in part analogous to the standard deviation of the lognormal distribution, and gamma value increases from -1 as the distribution matures and becomes more narrow. Sample

subpopulations were fit to this distribution; five subpopulations were required to account for over 95% of the variation noted for all samples.

4.1 PRE-SHOT SAMPLES

Those pre-shot samples analyzed were taken from radial distances of 15.8 m (0 - 0.8 m depth) and 25.9 m (0 - 1.8 m depth) along three principal radials (337, 225, and 270 degrees). The pre-shot desert-alluvium size characteristics are summarized in Table 1. Using normal statistics, the mean grain diameter averages 1.45 mm with a standard deviation of 0.65 (log units).

4.2 EJECTA AND FALLBACK SAMPLES

Ejecta and fallback were sampled and analyzed to a distance of 1000 m from SGZ along the same three radials as were pre-shot samples. The overall dispersal size characteristics are summarized by bulk sample (single population) lognormal statistics in Figure 5, for which a general increase in mean particle diameter is coupled to a decrease in standard deviation for samples taken at increasing distance. This coarsening and better sorting with distance is portrayed for each radial in Figures 6a and 6b; however, there is a marked variation in overall size characteristics of ejecta and fallback with azimuth.

To better characterize ejecta and fallback size characteristics, samples were decomposed into constituent subpopulations, because none of the samples are unimodal, the product of a single grain-size population. Subpopulations of the SFT distribution were best-fit to each sample by the method of Sheridan et al. (1986). In all samples 5 subpopulations were required to explain better than 95% of the observed variation. An important result plotted in Figure 7 is that the mode (peak size) of each subpopulation is fairly consistent for all samples with increasing distance from SGZ. Furthermore, Figure 7 includes subpopulation modes for pre-shot

samples (shown as <100 m), which also bear close resemblance to those of the ejecta samples. Note that subpopulation 5 (the silt fraction) is shown only for those samples subjected to centrifuge analysis. The weight fraction and gamma value (sorting) of each of these subpopulations varies with distance as shown in Figures 8a and 8b, in some cases showing marked inflections at about 500 m. In general, the abundance of subpopulation 5 is less than 6%, very nearly the same proportion noted in pre-shot samples. Note that in Figure 8a subpopulation 1 shows a rapid decrease in abundance out to 500 m beyond which it shows a strong increase; subpopulation 3 mimics the behavior of subpopulation 1 in a weak manner; conversely, subpopulation 2 increases markedly out to 500 m and then decreases thereafter; subpopulation 4 decrease linearly in abundance with distance. Gamma values in Figure 8b also show inflections at 400 to 600 m. The high gamma values for subpopulation 1 are somewhat biased in that the distribution could not be statistically analyzed for rocks bigger than a few centimeters; thus the subpopulation shows an artificial good sorting. Subpopulation 2 attains its lowest gamma value (broadest distribution) at medial ranges where it is also most abundant, whereas subpopulation 3 is better sorted where it is most abundant. Subpopulation 4 shows a distinct decrease in gamma with distance, indicating that it is becoming much more poorly defined as a subpopulation. Subpopulation 5 remains broad and poorly defined for all sample locations.

The azimuth effect upon subpopulation behavior is illustrated in Figures 9 and 10. Only subpopulations 2, 3, and 4 are considered because of bias, mentioned above, inherited from analytical method for the coarsest (subpopulation 1) and finest (subpopulation 5) modes. Figure 9 shows the marked difference in subpopulation abundances versus distance for the three analyzed radials. For radial 337 subpopulations 2 and 3 decrease with

distance, while they are generally increasing for radials 225 and 270. Radial 337 also shows an opposite behavior for subpopulation 4, increasing with distance while it drops to near zero abundance beyond 300 m for the other two radials. This opposite character of radial 337 is only shown for subpopulation 3 gamma values (Figure 10). Subpopulation 2 gamma values show a low at about 200-500 m for all radials where they are all most poorly defined in terms of central tendency or peakedness. Subpopulation 3 shows a decrease in gamma beyond 400 m, except for radial 337 where gamma increases markedly with distance (while subpopulation 3 becomes less abundant--Fig. 9b). In contrast subpopulation 4 gamma values decrease with distance along radial 337 as the subpopulations abundance increases. Much of the interpretation of these graphs is dependent upon corroborating observations, discussed later.

4.3 SWEEP-UP SAMPLES

Composites of the pre-shot desert alluvium and pre-shot DPR were analyzed in the same manner as were ejecta samples. While a composite of the desert alluvium (cobbles and pebbles removed) at 15.8 m from SGZ (0 - 0.8 m depth) shows a mean diameter of 0.895 mm and a standard deviation of 0.55, a composite (dry- and wet-sieved) of 24 samples (top 6.4 mm) of the DPR has a mean and standard deviation of 0.187 mm and 0.79, respectively. This difference reflects the fact that the pre-shot desert alluvium contained granules and pebbles not added to the DPR test bed. Overall, the same subpopulations are found in both, although in different abundances (Fig. 11).

Results of analysis of samples collected in the GREG/SNOB gages are shown in Figure 12. The HML sample (Fig. 12a) is significantly finer than the H-Tech samples. A very slight fining of composite 3 (Fig. 12c) relative to composite 2 (Fig. 12b) is observable, shown by an increase in subpopulation 4 abundance. Overall, the two H-Tech composite samples look

remarkably similar. A comparison of test bed and GREG/SNOB samples by subpopulations is summarized in Table 2.

5. DISCUSSION AND CONCLUSIONS

The results presented within this paper represent only partial analysis of the samples collected at the MISTY PICTURE test site. Furthermore, only a limited amount of time and effort has been made available to interpret the data so far acquired. Nevertheless, several conclusions can be drawn based upon the work to date.

To begin with, it is obvious from Figure 3 that mass/area of ejecta and fallout decreases with distance from SGZ. The effect of wind on ejecta distribution is also obvious in Figure 3. The radial that most closely follows wind direction, radial 270, has the greatest mass/area values near SGZ due to additional stem fallout loading along that radial. With increased distance from SGZ (>250 m) ejecta occurrence along all radials becomes more similar although the wind should also play a role in differentiating various subpopulations along different radials.

Second, the increase in mean particle size of ejecta with distance from SGZ for all radials (Figure 5a) in conjunction with better sorting (Figure 5b) suggests that different mechanisms control the distribution and sorting of particles within different environments relative to SGZ. For instance, the better sorting with increased particle size suggests that a ballistic transport mechanism is responsible for the accumulation of distal ejecta while poorly sorted, mixed size fractions proximal to SGZ are the result of multiple transport mechanisms.

The inflections in weight fraction percentages and gamma values for many subpopulations in the 400-600 m range suggest that a major change in dominance by a particular transport mechanism is occurring at this

distance. The decrease in subpopulation 1 to 500 m with an increase following 500 m suggests that the dominant mechanism affecting subpopulation 1 is ballistic transport, that ballistic transport becomes more dominant beyond the 500 m range, that particles affected by this transport mechanism are not heavily affected by wind direction, and that heterogeneity of the test bed is not a major factor in subpopulation 1 dispersal. However, the great variation seen among azimuths for the finer subpopulations (2-4), which is markedly illustrated by comparisons between Radial 337 and the other two radials, documents the potential effect of azimuths on ejecta/fallout occurrence. This is most likely as a result of both wind and starting materials (Figures 9 and 10). For instance, although subpopulation 2 shows very divergent weight fractions among the 3 radials (Figure 9), the gamma plots are very similar (Figure 10). This fact suggests that subpopulation 2 was responding to a similar transport mechanism that controlled its sorting, that accumulation of subpopulation 2 may have been influenced by wind, and that the occurrence of subpopulation 2 in the ejecta was heavily influenced by its abundance in the pre-shot materials.

Subpopulations 3 and 4 represent fine ejecta materials with modes between approximately 0.1 and 0.7 mm. Figure 9 shows that along radial 337 these subpopulations strongly increase with distance, whereas along the other two radials they generally decrease (with exception to subpopulation 3 along radial 225). Observation of wet aggregation of fine materials into larger clumps of ejecta along radial 337 suggests that the reason this radial shows an increase in abundances of subpopulation 3 and 4 is the addition of aggregated fines from finer subpopulations. This possibility is especially true for subpopulation 3, which becomes better sorted with distance along radial 337 (Fig. 10b).

The same 5 subpopulations are present in the composite samples taken from the test bed as are found in all post-shot ejecta and fallout samples (Figure 7). Weight fractions of the subpopulations in post-shot samples may vary greatly, but the fingerprint of the starting materials is always present. Transport models that consider all possible mechanisms, while taking into account asymmetrical aberrations such as wind, should be able to (1) predict the occurrence of particle distributions following the shot throughout the test site, based on test bed data, or (2) based on ejecta/fallout data, define starting test bed heterogeneities. Overall we note the fact that subpopulation 5, fine dust less than 45 microns in diameter (average about 4-8 microns for analyzed samples) is about as abundant in the ejecta as in the starting materials. With this information and knowledge of the ejecta and crater volume the abundance of fine dust injected into the atmosphere can be calculated.

Variations in the materials collected in the GREG/SNOB gages located in the DPR also fit into a predictive scheme. In general, the same subpopulations were present in the pre-shot alluvium as occurred in the DPR pre-test bed. The HML sample is significantly finer than the H-Tech samples, probably because the HML gage sampled along inclined planes rather than parallel to the ground surface as did the H-Tech gages. The fining in H-Tech composite 3 relative to composite 2 can be attributed to its higher sampling height compared to composite 2. Thus, the subpopulations found in the gages have been inherited from the test bed and only vary with respect to gage location.

6.ACKNOWLEDGMENTS

This work was sponsored by the Defense Nuclear Agency under IACRO 87-832, task code and title: RA/RJ, Aircraft Systems V&H, work unit code and title: 00073, Test Debris Exam, work unit manager: Lt. Col. R. Adams.

We also acknowledge the support of Dr. Charles Galloway, DNA/SPWE, Dr. Allen S. Mason, and his co-workers at the Los Alamos National Laboratory, and the Test Group Director, Maj. Greg Walls, USA, and his staff at the White Sands Missile Range.

We are grateful for Drs. Noel Ethridge of the Aberdeen Research Center and Bruce Hartenbaum of H-Tech for providing sweep-up samples.

This work was partially funded under the auspices of the United States Department of Energy under contract W-7405-ENG-36.

7. REFERENCES

Bayhurst, G.K., D.L. Finnegan, R.C. Hagan, A.S. Mason, E.J. Mroz, C.L. Peach, R. Raymond, Jr.,and K.H. Wohletz, 1988: Misty Picture Dust and Fallout Characterization, Los Alamos National Laboratory Report LA-CP-88-1, submitted to the MISTY PICTURE Results Symposium, Harry Diamond Lab., Adelphi, Maryland, 30 pgs.

Benson, K. et al., 1988: Cratering and Related Effects for the MISTY PICTURE Event, NMERI WA6 (6.03), March 1988.

Brown, W.K., 1986: Comparison of a Theory of Sequential Fragmentation with the Initial Mass Function of Stars, Astrophysics and Space Sci., 122, 287-298.

Brown, W.K., in press: A Theory of Sequential Fragmentation and Its Astronomical Applications, submitted to J. of Astrophysics and Astron.

Mason, A.S., Finnegan, D.L., Hagan, R.C., Raymond, R.Jr., Cocks, G.G., Zoller, W.H., and Peach, C.L., 1987: Lofting of Dust by Very Large Explosions, Los Alamos Manuscript LA-11080-MS, 14 pgs.

Phillips, B., 1987: Memorandum for : Director, Defense Nuclear Agency - Subject: Surficial Soil Data Collected on the MISTY PICTURE DPR, 14 July, 1987.

Rawson, G., 1987a: Analysis of MISTY PICTURE Sweep-up Dust (Trapped in 2 HML Models -- Greg/Snob Ports), RDA Consultant presentation at BMO, 6 Oct., 1987.

Rawson, G., 1987b: Analysis of MISTY PICTURE Sweep-up Dust (Trapped in Greg/Snob gage Ports -- 25 to 80 psi) RDA Consultant, presented at the Harry Diamond Lab., Adelphi, Maryland.

Scott, S., in progress: Crater Ejecta Missle Survey for the MISTY PICTURE Event, WES Tech. Paper.

Sheridan, M.F., K.H. Wohletz, and J. Dehn, 1986: Discrimination of Grain Size Subpopulations in Pyroclastic Deposits, Geology, 15, 367-370.
Wisotski, J., 1987: MISTY PICTURE Artificial Ejecta, DNA Experiment 8242 SAIC Subcontract, Denver Research Institute, Report 5-33138.
Wohletz, K.H., M.F. Sheridan, and W.K. Brown, 1987: Sequential Fragmentation: A New Model for Analysis of Size Distributions, Geol. Soc. Amer. Abst. w/ Progs. 19:7, 894.
Wohletz, K.H., M.F. Sheridan, and W.K. Brown, in press: Particle Size Distributions and the Sequential Fragmentation/Transport Theory Applied to Volcanic Ash, submitted to J. Geophys. Res.

Table 1. Particle-size characteristics of pre-shot desert alluvium fit to the SFT distribution*

Subpopulation	Mode (mm)	Gamma (γ)	Weight Fraction
1	9.707	2.36	0.29
2	2.197	-0.85	0.36
3	0.636	-0.47	0.16
4	0.185	-0.25	0.14
5	0.066	-0.28	0.04

* Data obtained by dry-sieving and centrifugal settling techniques. SFT (sequential fragmentation/transport) distribution of Wohletz et al. (1987) is similar to the lognormal distribution and is applied to subpopulations found to comprise each sample. The mode is the peak location of each subpopulation, and gamma is analogous to the standard deviation where better sorting (narrower distribution) is obtained with increasing gamma. Subpopulations 1 and 5 are somewhat biased by analytical technique, such that subpopulation 1 at nearly 10 mm includes larger pebbles and cobbles, while subpopulation 5, the silt fraction, might for some samples be near the 10 to 20 micron size, as determined by centrifuge.

Table 2. Comparison of test bed and GREG/SNOB samples by subpopulation

Subpopulation	Pre-shot Alluvium	DPR Radial*	Comp. 1 (HML)	Comp. 2 (1-9")	Comp. 3 (12-60")
Modes (mm)					
1	4.595	4.000 (3.031)	0.953	1.516	2.809
2	1.414	1.414 (0.683)	0.599	0.616	0.599
3	0.574	0.660 (0.177)	0.165	0.189	0.189
4	0.227	0.177 (0.046)	0.085	0.072	0.069
5	0.077	0.046 (0.011)	0.008	0.015	0.015
Weight Fraction					
1	0.27	0.10 (0.14)	0.03	0.05	0.07
2	0.31	0.06 (0.25)	0.11	0.18	0.16
3	0.18	0.24 (0.34)	0.58	0.38	0.33
4	0.21	0.32 (0.20)	0.28	0.32	0.41
5	0.04	0.21 (0.04)	0.01	0.05	0.03
Gamma					
1	-0.78	-0.78 (-0.86)	-0.69	-0.86	-0.49
2	-0.80	-0.80 (-0.60)	-0.76	-0.76	-0.82
3	-0.70	-0.60 (-0.80)	-0.88	-0.92	-0.9?
4	-0.80	-0.77 (-0.57)	-0.70	-0.83	-0.85
5	-0.70	-0.60 (-0.60)	-0.80	-0.87	-0.87

* Subpopulation statistics for the DPR radial were calculated first to reflect coarse modes present in the pre-shot alluvium and then in parentheses to reflect finer modes concentrated in the upper 6 mm of the DPR test bed, materials lofted and sampled by the GREG/SNOB gages.

FIGURE CAPTIONS

1. Map showing location of pre-shot samples taken from the MISTY PICTURE Test Bed.

2. Map showing location of post-shot samples collected within 1000 m of MISTY PICTURE SGZ.

3. Plot of grams/sq. m vs. distance from SGZ for ejecta collected along the 225, 270, and 337 radials. Radial 270, being nearly downwind from SGZ, has a greater mass/area of ejecta near SGZ due to additional stem fallout loading.

4. Cross-section of the crater resulting from the MISTY PICTURE shot along the 220 radial. Fallback sample locations are shown at 60 m and 67 m from SGZ.

5. Plot of ejecta, bulk-sample, mean particle diameters and standard deviation versus distance. The polynomial best-fit shown illustrates general behavior of sample data with increasing distance from SGZ (distance = 0 m). Samples generally increase in mean particle diameter and decrease in standard deviation with increasing distance from the crater. Note that the standard deviations are given in logarithmic units which pertain to lognormal (gaussian) statistics.

6. Plots showing the variation in mean and standard deviation of particle diameters with distance and azimuth designated as radials 337, 225, and 270. A) Mean diameters along all radials generally increase with distance, except for an initial decrease noted for radial 225 at distances less than 300 m and a decrease along radial 337 at distances greater than approximately 700 m B) Standard deviations along all three radials decrease with distance, showing that bulk samples are better sorted (have a narrower distribution with greater central tendency) with distance.

7. Plot of sample subpopulation mode (distribution peak) with increasing distance. In this plot, data from pre-shot alluvium samples, taken within the area cratered (distance $<$ 100 m), are included with ejecta sample data. Five subpopulations were required to explain over 95 % of distribution variances for each sample. Nearly the same subpopulation mode is present in all samples, indicating that the ejecta distributions inherited subpopulations from the pre-shot materials. Note that values for subpopulation 5 (the finest) are shown only for those samples analyzed along radial 337, but we consider these to be representative of all samples.

8. Plots showing subpopulation weight-fraction and gamma values (analogous to standard deviation) as a function of distance. Data are simplified by polynomial curves best-fit to each subpopulation and include only ejecta samples; data obtained by sequential fragmentation/transport (SFT) analysis. Compare these data to those listed in Table 1 to see variation between pre-shot and ejecta samples. A) Weight fractions of subpopulation 5 are small, generally less than 6 %, so that the other 4 subpopulations make up the bulk of ejecta samples. B) Gamma values for the five subpopulations vary with distance; those of subpopulation 5 are for only those samples analyzed along radial 337. Gammas for subpopulation 1

(coarsest subpopulation) are biased towards higher values because its distribution is not completely analyzed to diameters greater than 12 mm.

9. Weight-fraction plots of subpopulations 2, 3, and 4 versus distance and azimuth; data represented by best-fit polynomial curves. A) Subpopulation 2 (approximately 2-mm diameter) shows a general increase along radials 225 and 270 but a decrease along radial 337. B) Subpopulation 3 (approximately 0.6-mm diameter) shows similar trends with distance as subpopulation 2. C) Subpopulation 4 (approximately 0.1-mm diameter) shows a marked increase along radial 337 and general decrease along the other radials in contrast to subpopulations 2 and 3.

10. Gamma plots of subpopulations 2, 3, and 4 versus distance and azimuth; data represented by best-fit polynomial curves. A) Subpopulation 2 shows a general increase in gamma values with distance for all radials at distances greater than about 500 m, signifying that the distribution tends towards better sorting. B) Subpopulation 3 shows that samples from radial 337 (gamma increasing with distance) contrast with those from the other radials. C) Subpopulation 4 gamma values markedly decrease with distance in contrast with values for the other radials. The distinction of subpopulations 3 and 4 for radial 337 is attributed to fines aggregation that could broaden the distribution of 4 while narrowing that of subpopulation 3.

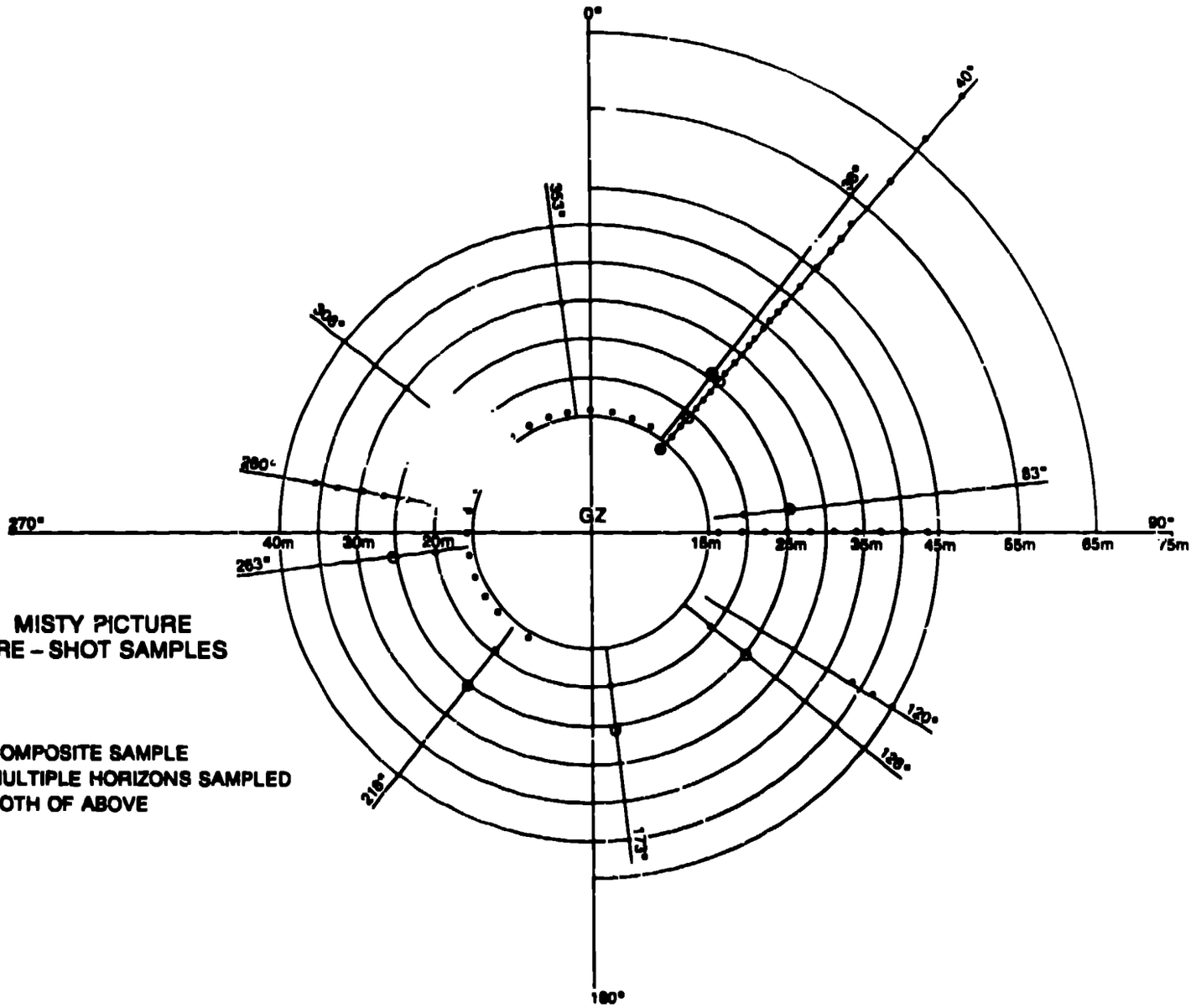

MISTY PICTURE
PRE – SHOT SAMPLES

- COMPOSITE SAMPLE
- MULTIPLE HORIZONS SAMPLED
- BOTH OF ABOVE

Figure 1

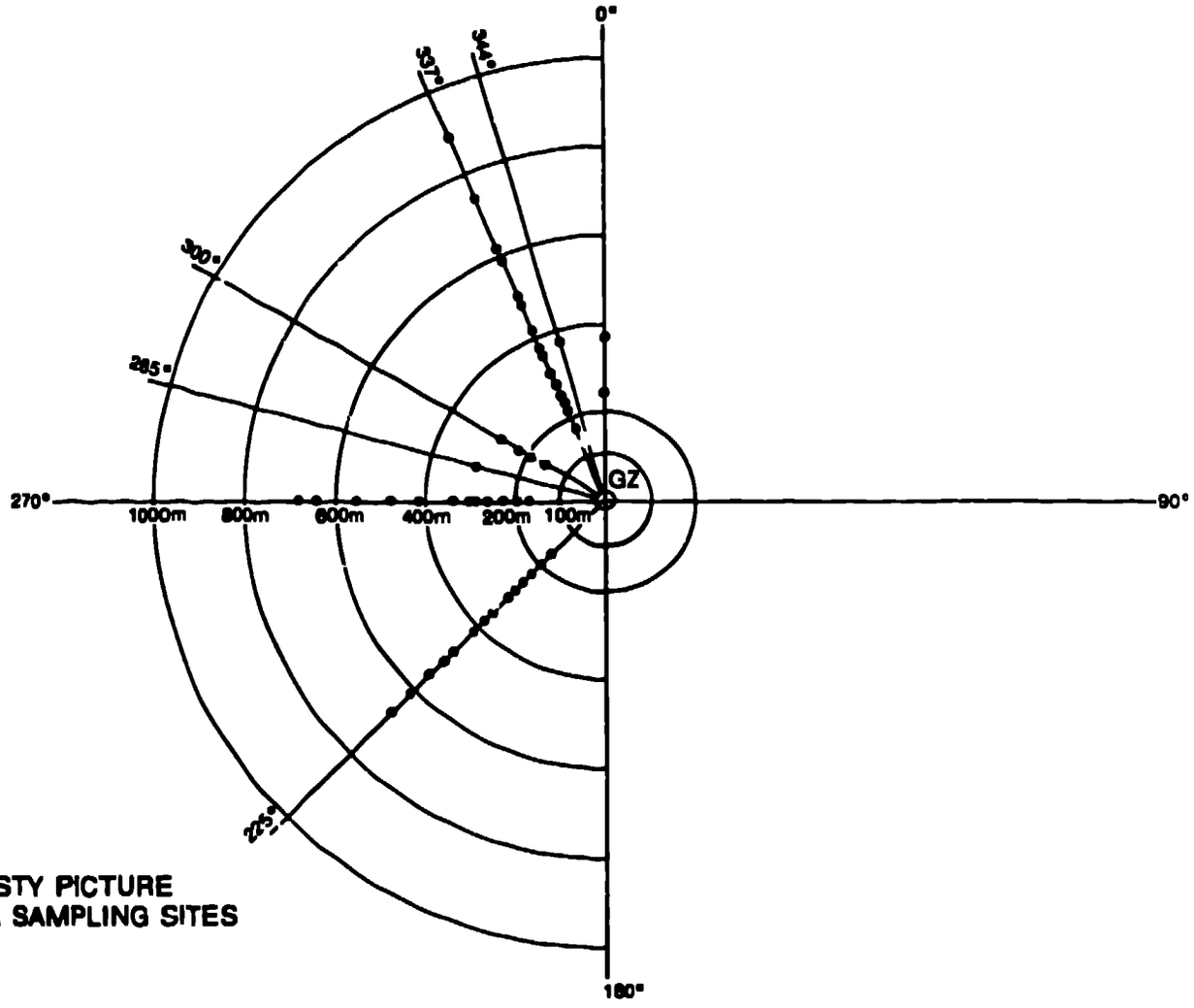

MISTY PICTURE
EJECTA SAMPLING SITES

Figure 2

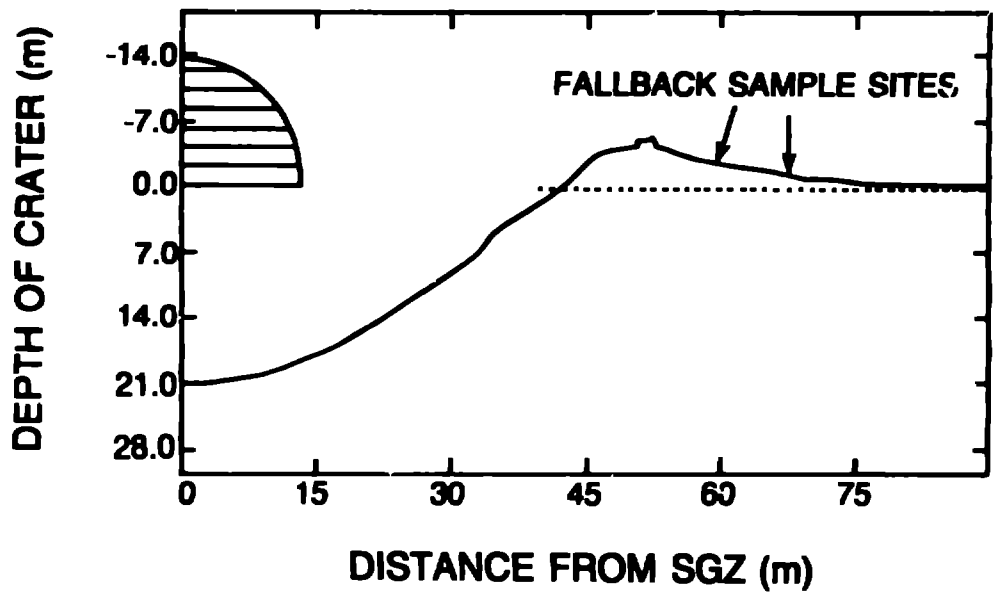
DEPTH OF CRATER (m)
-14.0
-7.0
0.0
7.0
14.0
21.0
28.0
FALLBACK SAMPLE SITES
0
15
30
45
60
75
DISTANCE FROM SGZ (m)

Figure 4

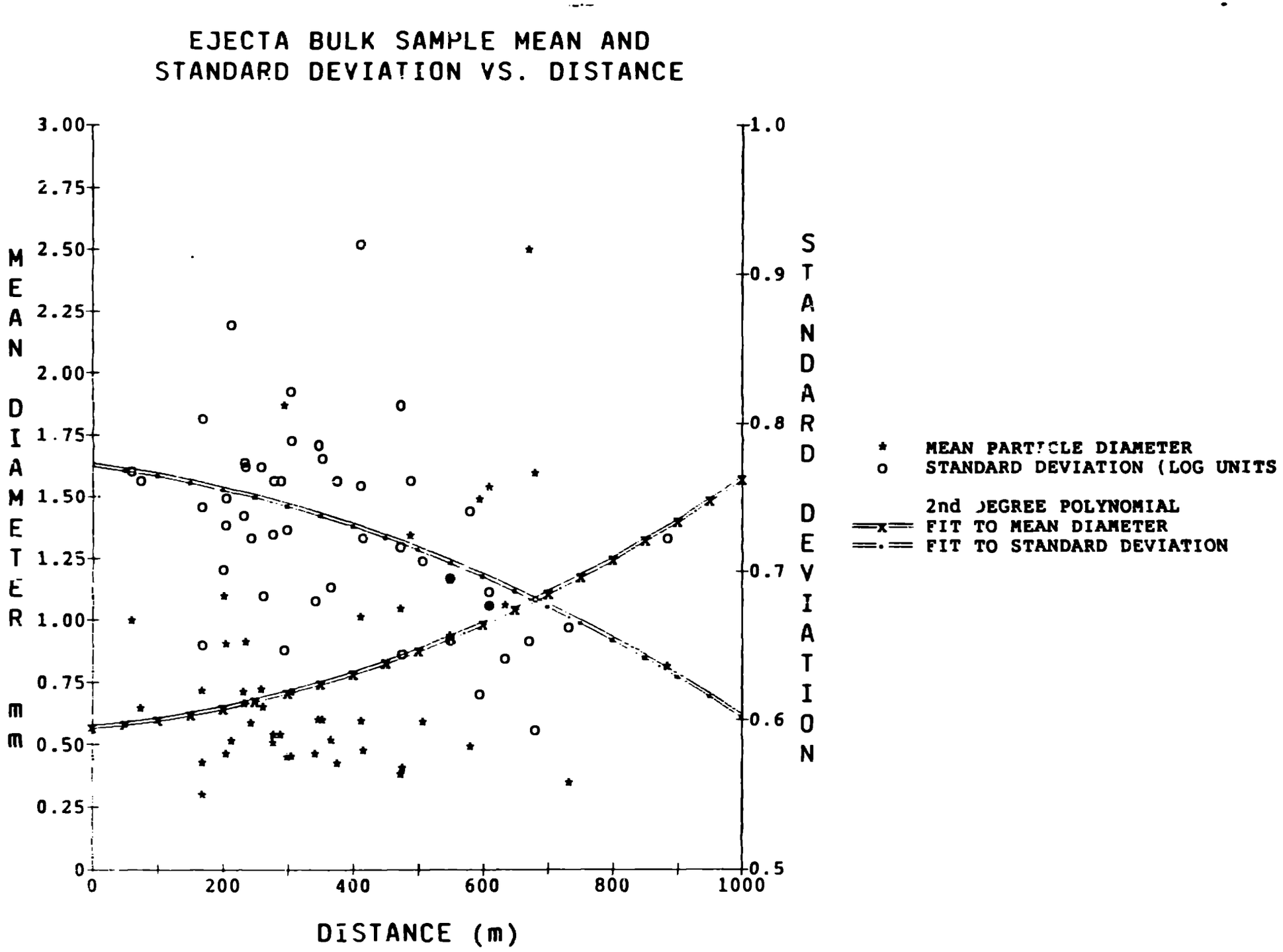
EJECTA BULK SAMPLE MEAN AND
STANDARD DEVIATION VS. DISTANCE
MEAN DIAMETER mm
STANDARD DEVIATION
DISTANCE (m)
3.00
2.75
2.50
2.25
2.00
1.75
1.50
1.25
1.00
0.75
0.50
0.25
0
1.0
0.9
0.8
0.7
0.6
0.5
0
200
400
600
800
1000
MEAN PARTICLE DIAMETER
STANDARD DEVIATION (LOG UNITS
2nd DEGREE POLYNOMIAL
FIT TO MEAN DIAMETER
FIT TO STANDARD DEVIATION

Figure 5

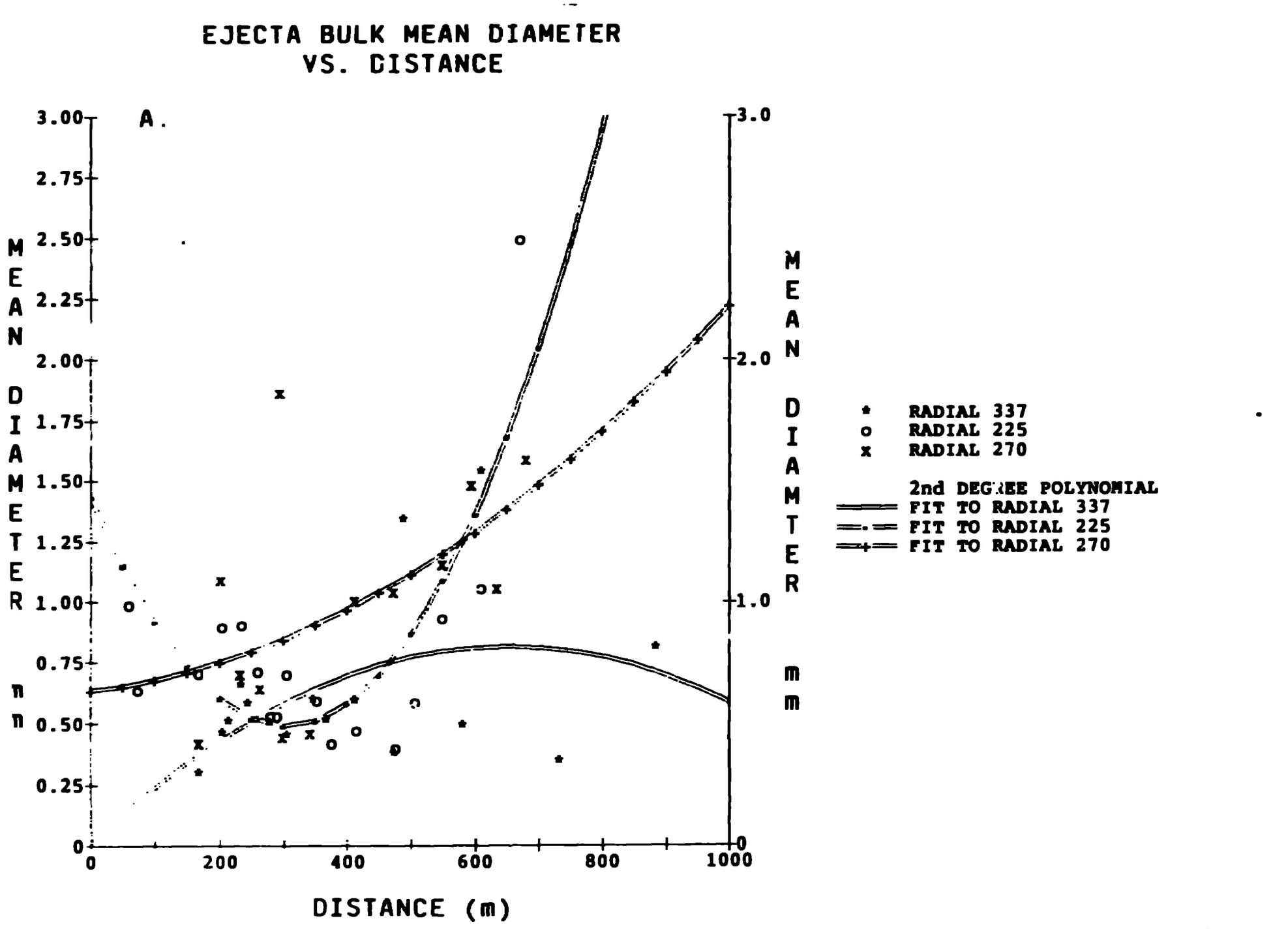
EJECTA BULK MEAN DIAMETER
VS. DISTANCE
A.
MEAN DIAMETER mm
3.00
2.75
2.50
2.25
2.00
1.75
1.50
1.25
1.00
0.75
0.50
0.25
0
3.0
2.0
1.0
0
MEAN DIAMETER mm
0
200
400
600
800
1000
DISTANCE (m)
RADIAL 337
RADIAL 225
RADIAL 270
2nd DEGREE POLYNOMIAL
FIT TO RADIAL 337
FIT TO RADIAL 225
FIT TO RADIAL 270

Figure 6a

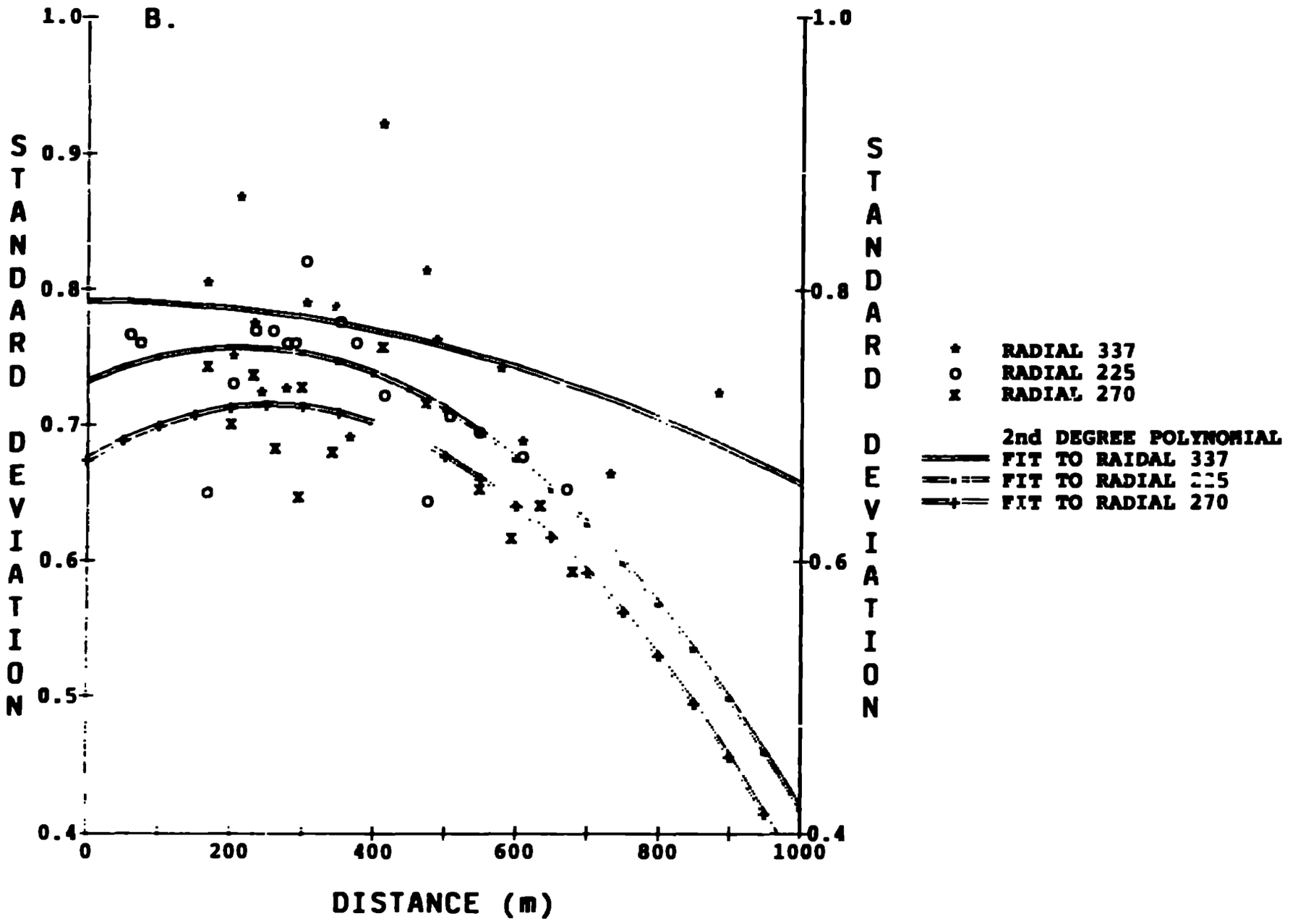
EJECTA BULK SAMPLE STANDARD DEVIATION
VS. DISTANCE
B.
STANDARD DEVIATION
1.0
0.9
0.8
0.7
0.6
0.5
0.4
0
200
400
600
800
1000
DISTANCE (m)
RADIAL 337
RADIAL 225
RADIAL 270
2nd DEGREE POLYNOMIAL
FIT TO RAIDAL 337
FIT TO RADIAL 225
FIT TO RADIAL 270

Figure 6b

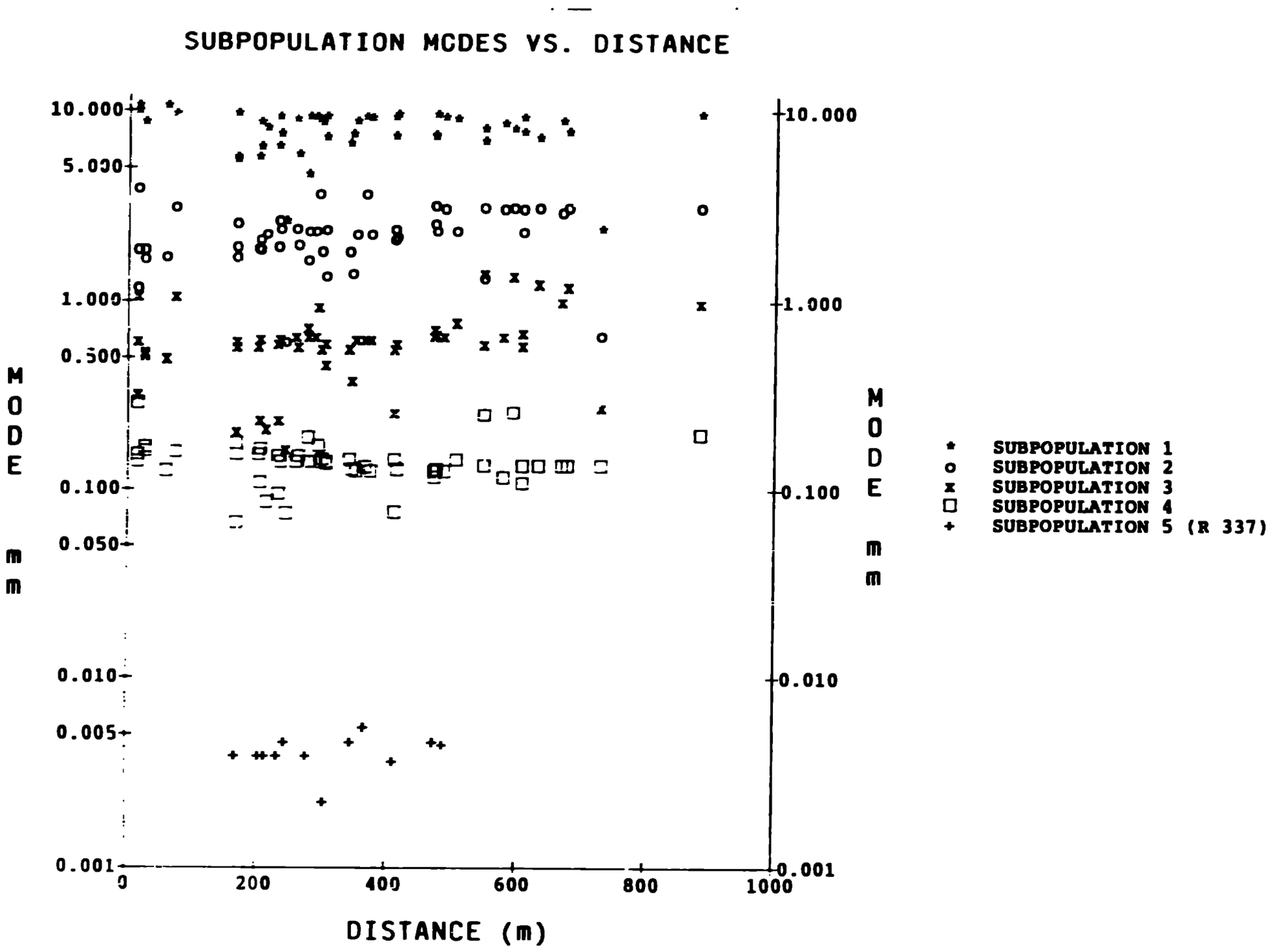
SUBPOPULATION MODES VS. DISTANCE
MODE mm
10.000
5.000
1.000
0.500
0.100
0.050
0.010
0.005
0.001
0
200
400
600
800
1000
DISTANCE (m)
SUBPOPULATION 1
SUBPOPULATION 2
SUBPOPULATION 3
SUBPOPULATION 4
SUBPOPULATION 5 (R 337)

Figure 7

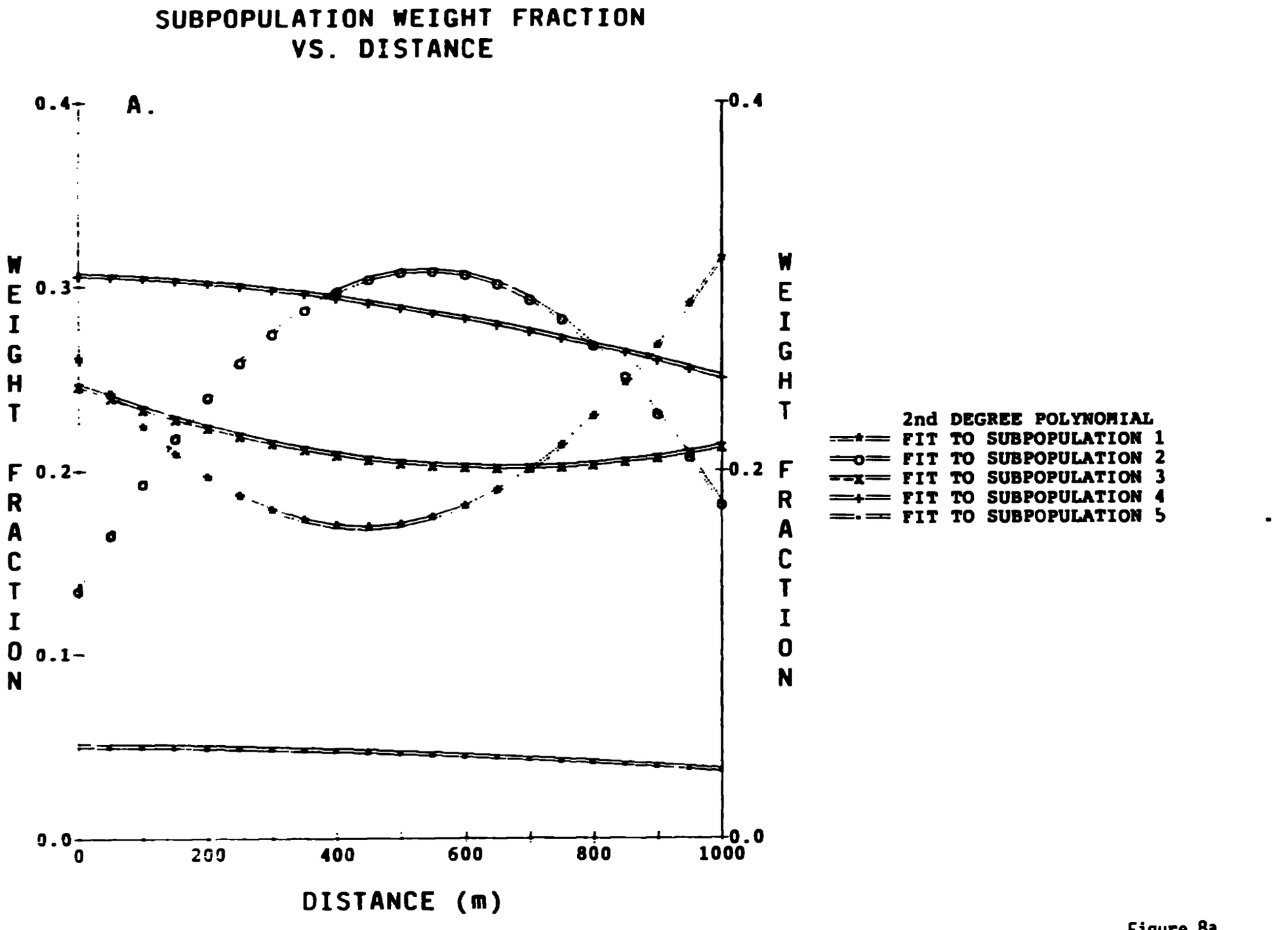
SUBPOPULATION WEIGHT FRACTION
VS. DISTANCE
A.
WEIGHT FRACTION
0.4
0.3
0.2
0.1
0.0
0
200
400
600
800
1000
DISTANCE (m)
2nd DEGREE POLYNOMIAL
FIT TO SUBPOPULATION 1
FIT TO SUBPOPULATION 2
FIT TO SUBPOPULATION 3
FIT TO SUBPOPULATION 4
FIT TO SUBPOPULATION 5

Figure 8a

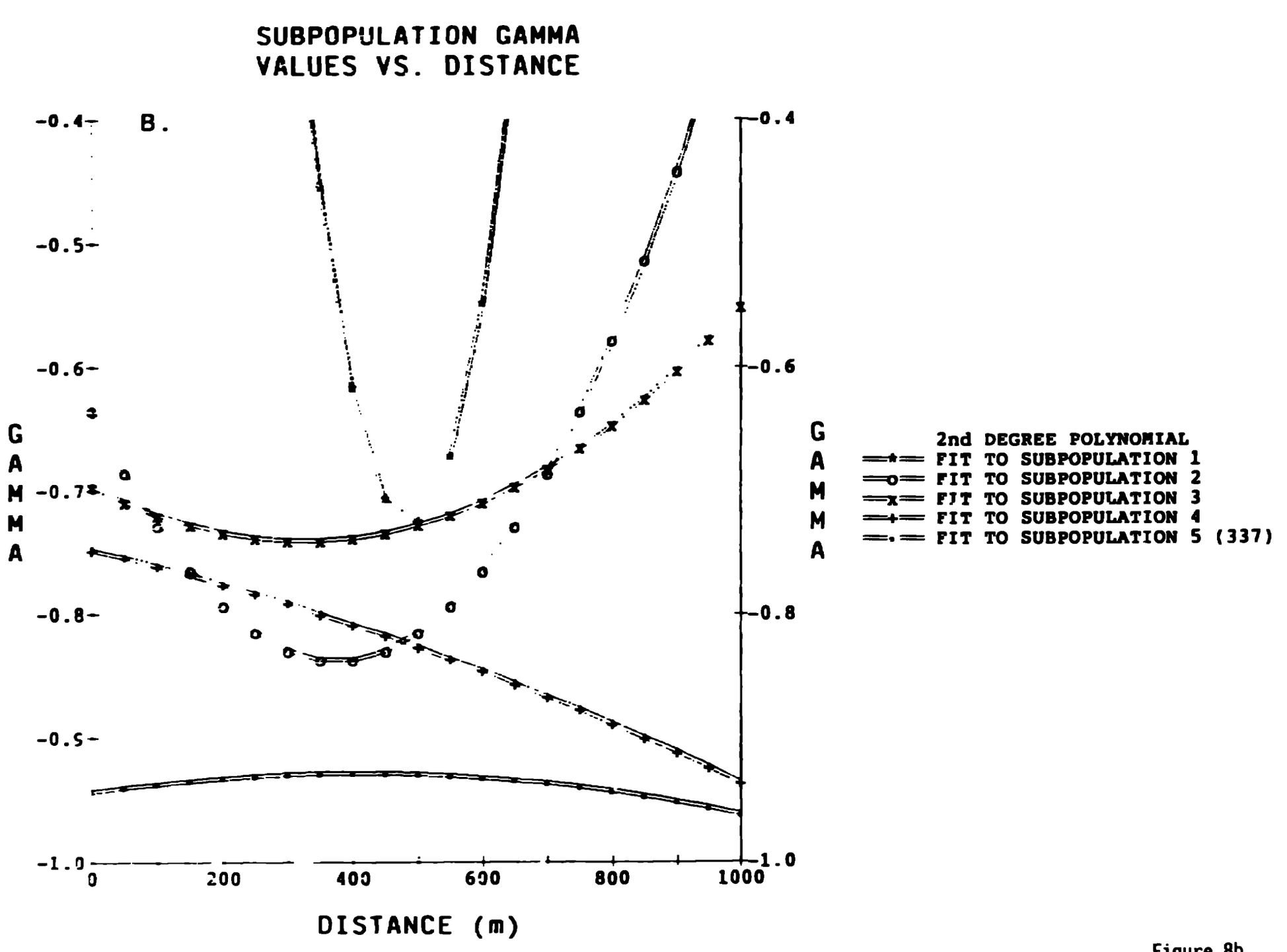
SUBPOPULATION GAMMA
VALUES VS. DISTANCE
B.
-0.4
-0.5
-0.6
-0.7
-0.8
-0.9
-1.0
0.4
0.6
0.8
1.0
0
200
400
600
800
1000
DISTANCE (m)
GAMMA
GAMMA
2nd DEGREE POLYNOMIAL
FIT TO SUBPOPULATION 1
FIT TO SUBPOPULATION 2
FIT TO SUBPOPULATION 3
FIT TO SUBPOPULATION 4
FIT TO SUBPOPULATION 5 (337)

Figure 8b

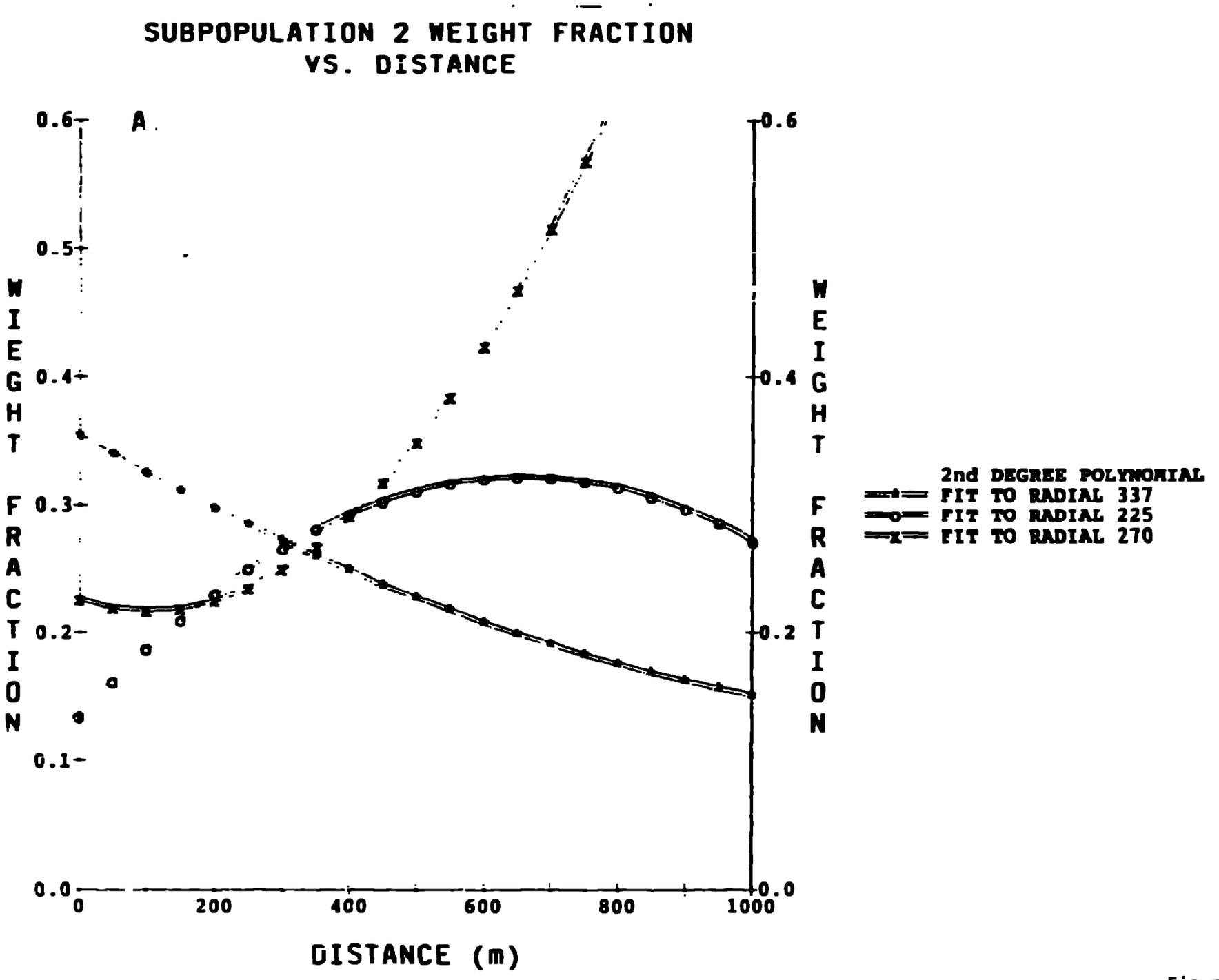
SUBPOPULATION 2 WEIGHT FRACTION
VS. DISTANCE
A
WEIGHT FRACTION
0.6
0.5
0.4
0.3
0.2
0.1
0.0
0
200
400
600
800
1000
DISTANCE (m)
2nd DEGREE POLYNOMIAL
FIT TO RADIAL 337
FIT TO RADIAL 225
FIT TO RADIAL 270

Figure 9a

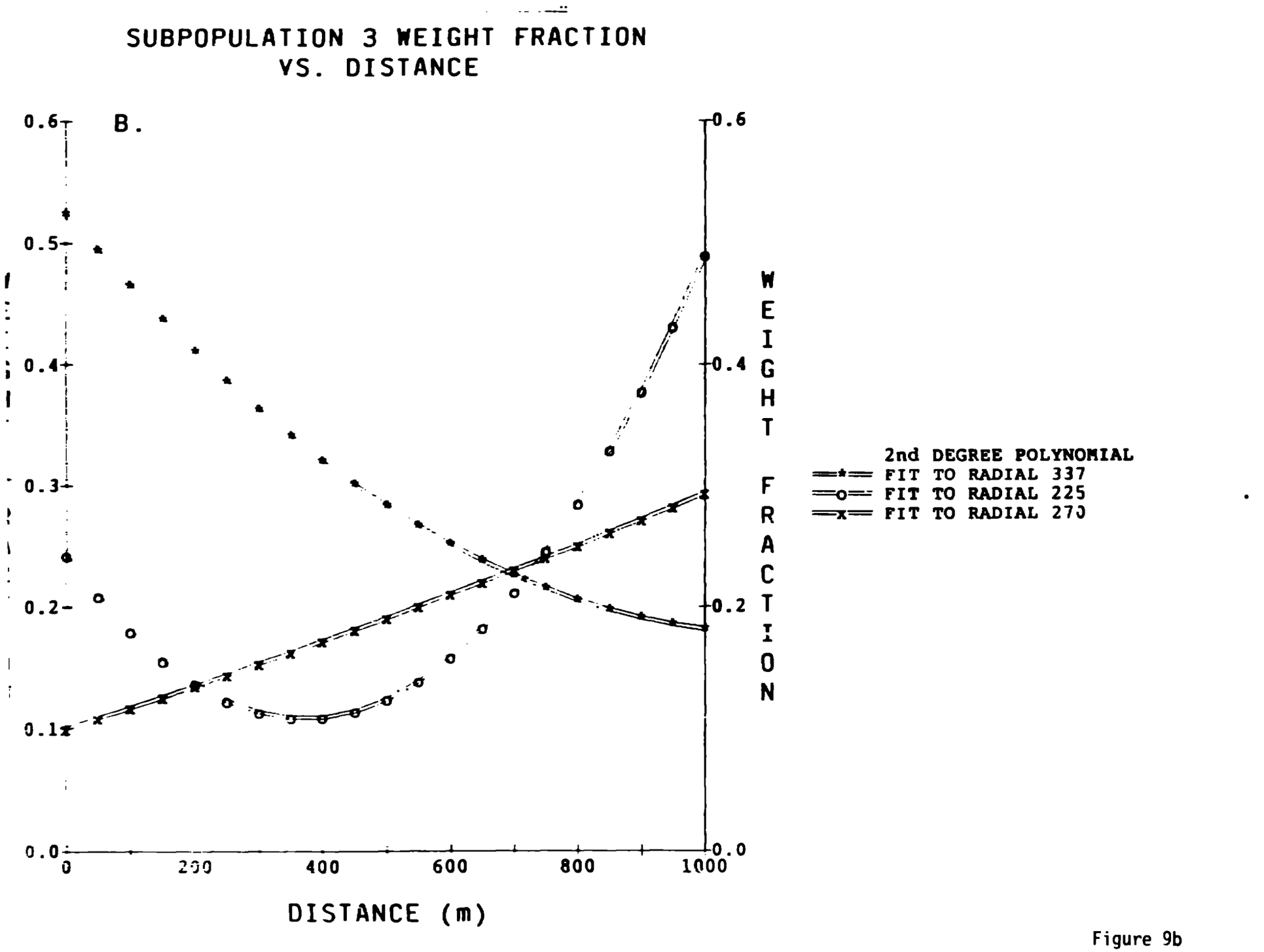
SUBPOPULATION 3 WEIGHT FRACTION
VS. DISTANCE
B.
0.6
0.5
0.4
0.3
0.2
0.1
0.0
0
200
400
600
800
1000
DISTANCE (m)
WEIGHT FRACTION
2nd DEGREE POLYNOMIAL
FIT TO RADIAL 337
FIT TO RADIAL 225
FIT TO RADIAL 270

Figure 9b

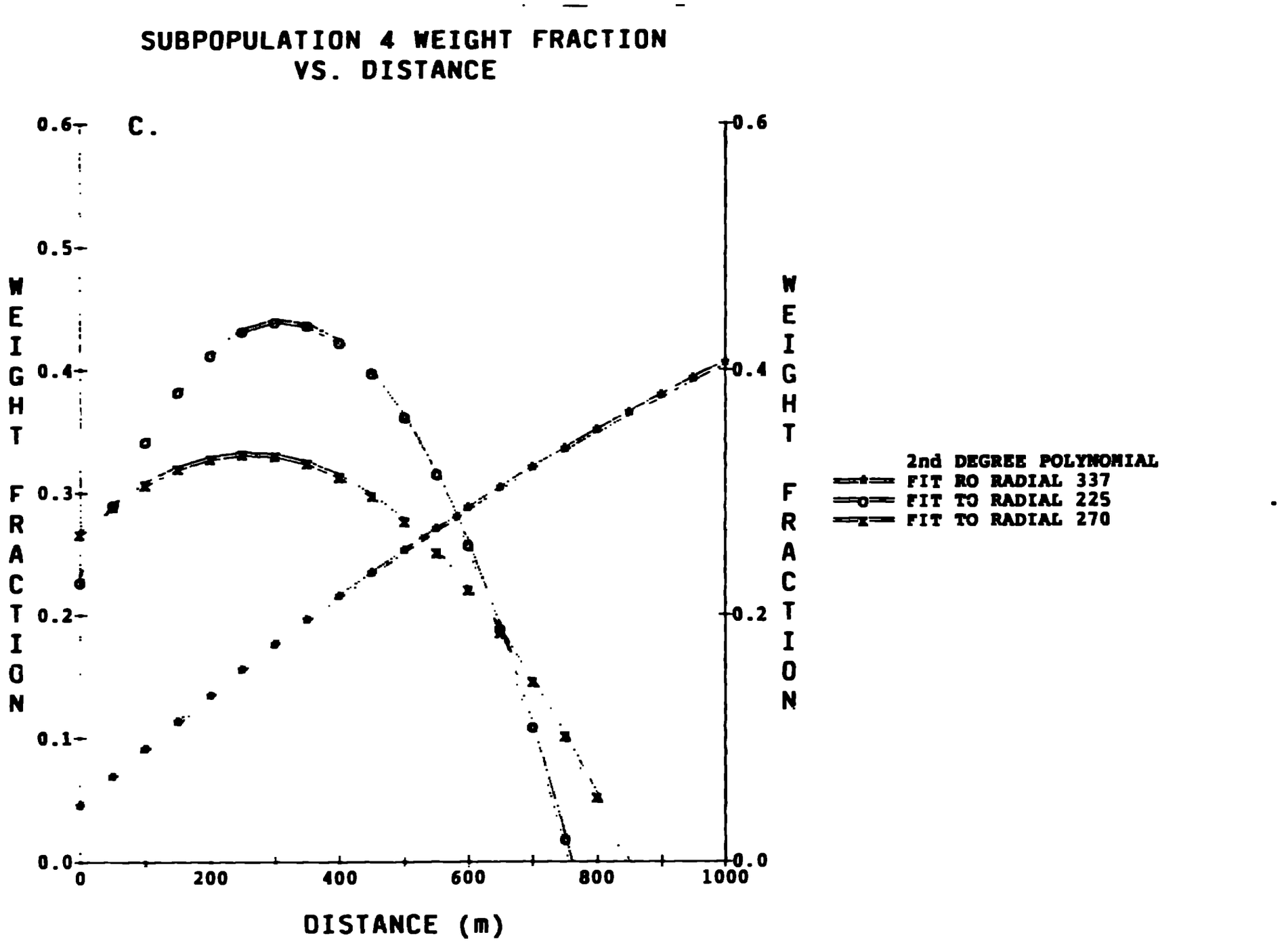
SUBPOPULATION 4 WEIGHT FRACTION
VS. DISTANCE
C.
WEIGHT FRACTION
0.6
0.5
0.4
0.3
0.2
0.1
0.0
0
200
400
600
800
1000
DISTANCE (m)
2nd DEGREE POLYNOMIAL
FIT RO RADIAL 337
FIT TO RADIAL 225
FIT TO RADIAL 270

Figure 9c

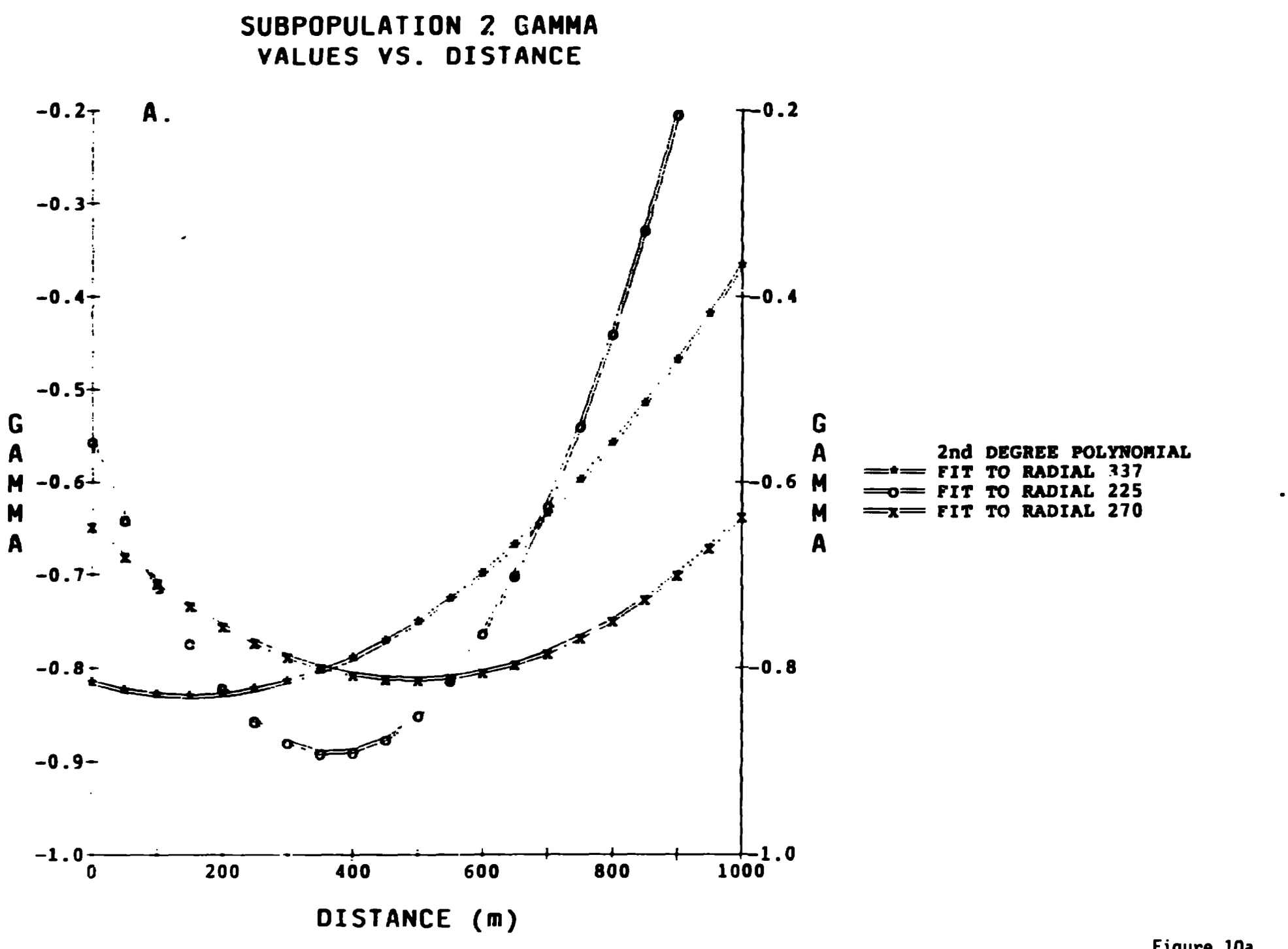
SUBPOPULATION 2 GAMMA
VALUES VS. DISTANCE
A.
-0.2
-0.3
-0.4
-0.5
-0.6
-0.7
-0.8
-0.9
-1.0
0.2
0.4
0.6
0.8
1.0
GAMMA
GAMMA
0
200
400
600
800
1000
DISTANCE (m)
2nd DEGREE POLYNOMIAL
FIT TO RADIAL 337
FIT TO RADIAL 225
FIT TO RADIAL 270

Figure 10a

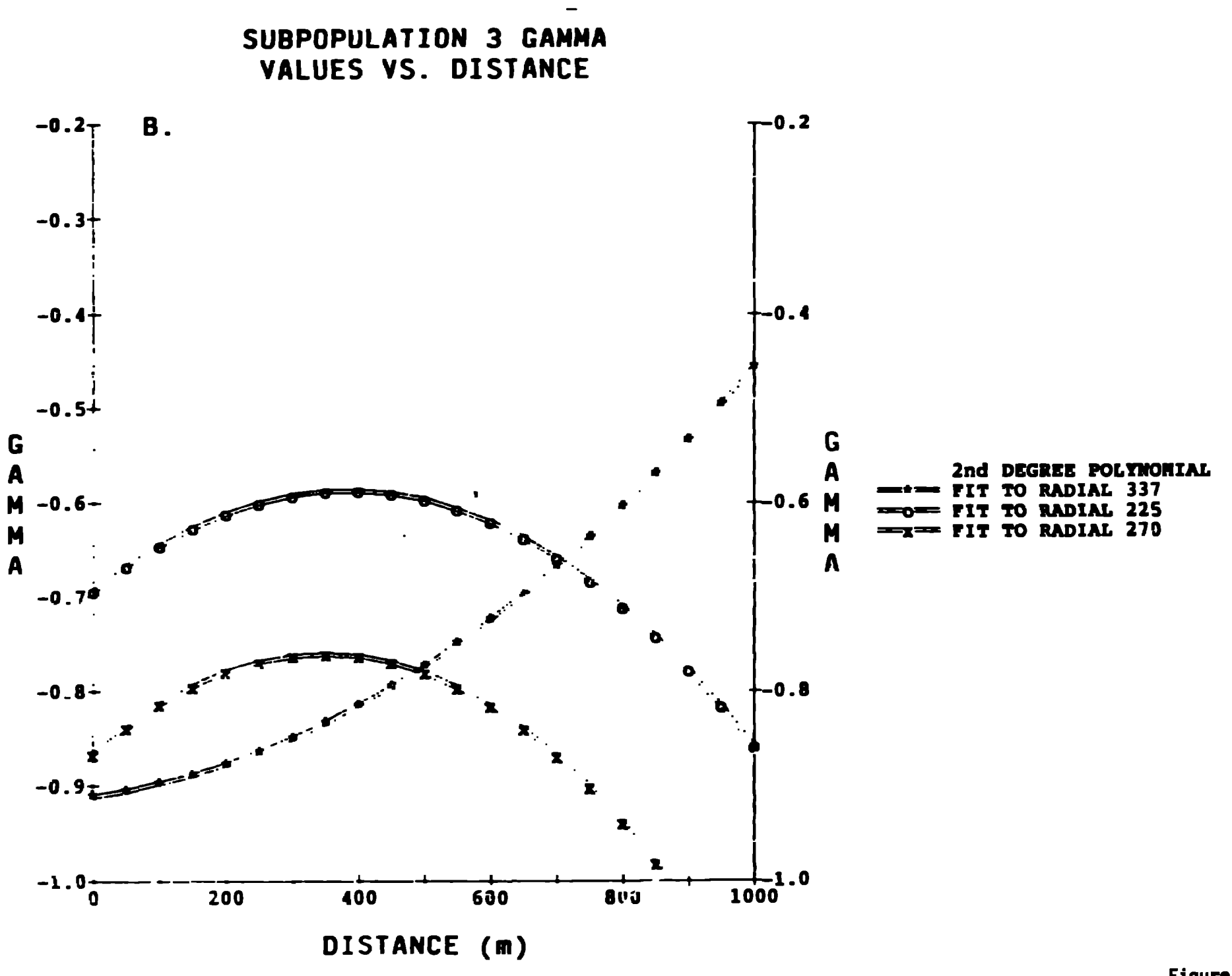
SUBPOPULATION 3 GAMMA
VALUES VS. DISTANCE
B.
-0.2
-0.3
-0.4
-0.5
-0.6
-0.7
-0.8
-0.9
-1.0
0.2
0.4
0.6
0.8
1.0
GAMMA
GAMMA
0
200
400
600
800
1000
DISTANCE (m)
2nd DEGREE POLYNOMIAL
FIT TO RADIAL 337
FIT TO RADIAL 225
FIT TO RADIAL 270

Figure 10b

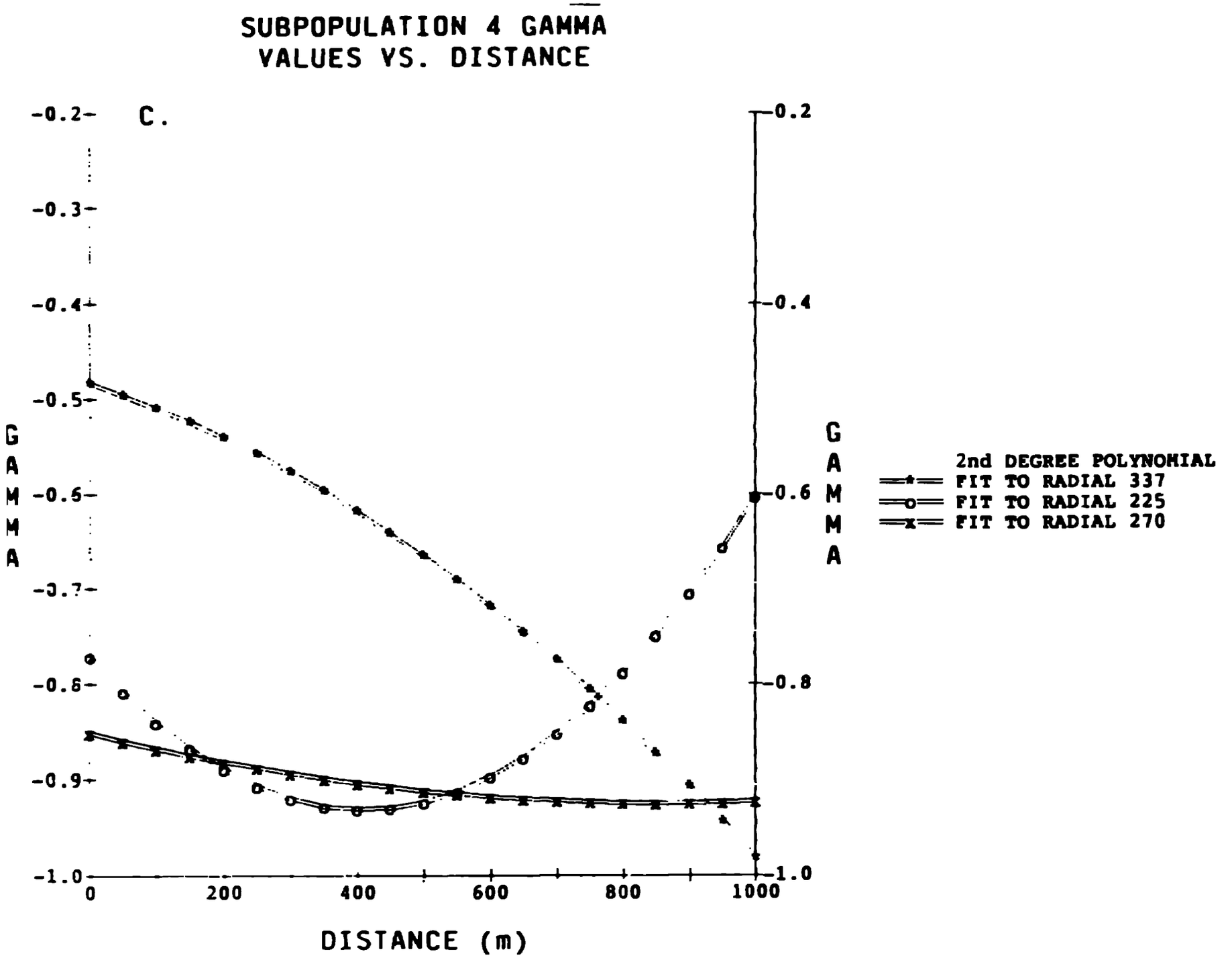
SUBPOPULATION 4 GAMMA
VALUES VS. DISTANCE
C.
-0.2
-0.3
-0.4
-0.5
-0.6
-0.7
-0.8
-0.9
-1.0
0.2
0.4
0.6
0.8
1.0
GAMMA
GAMMA
0
200
400
600
800
1000
DISTANCE (m)
2nd DEGREE POLYNOMIAL
FIT TO RADIAL 337
FIT TO RADIAL 225
FIT TO RADIAL 270

Figure 10c

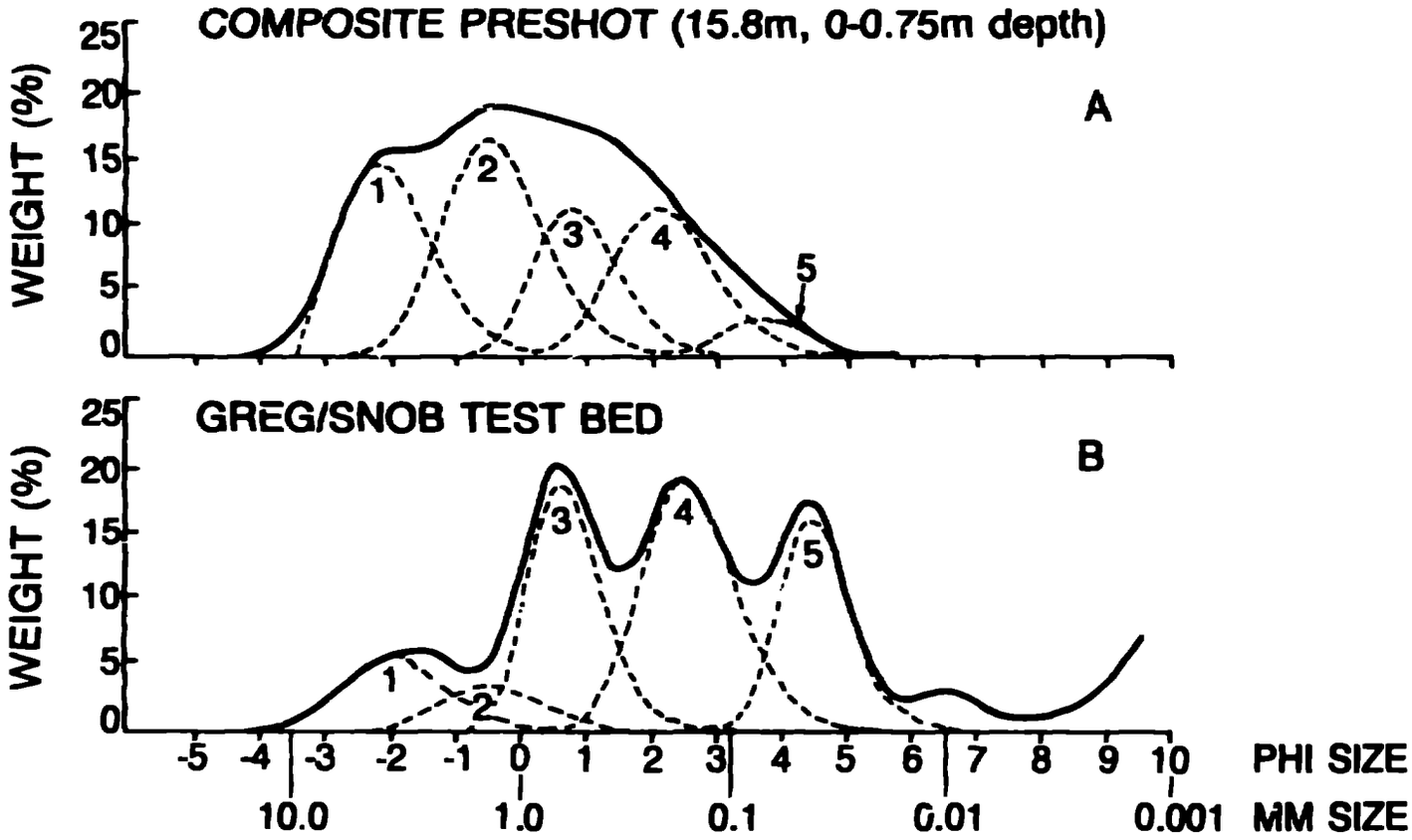
COMPOSITE PRESHOT (15.8m, 0-0.75m depth)
A
WEIGHT (%)
25
20
15
10
5
0
1
2
3
4
5
GREG/SNOB TEST BED
B
WEIGHT (%)
-5 -4 -3 -2 -1 0 1 2 3 4 5 6 7 8 9 10
PHI SIZE
10.0 1.0 0.1 0.01 0.001
MM SIZE

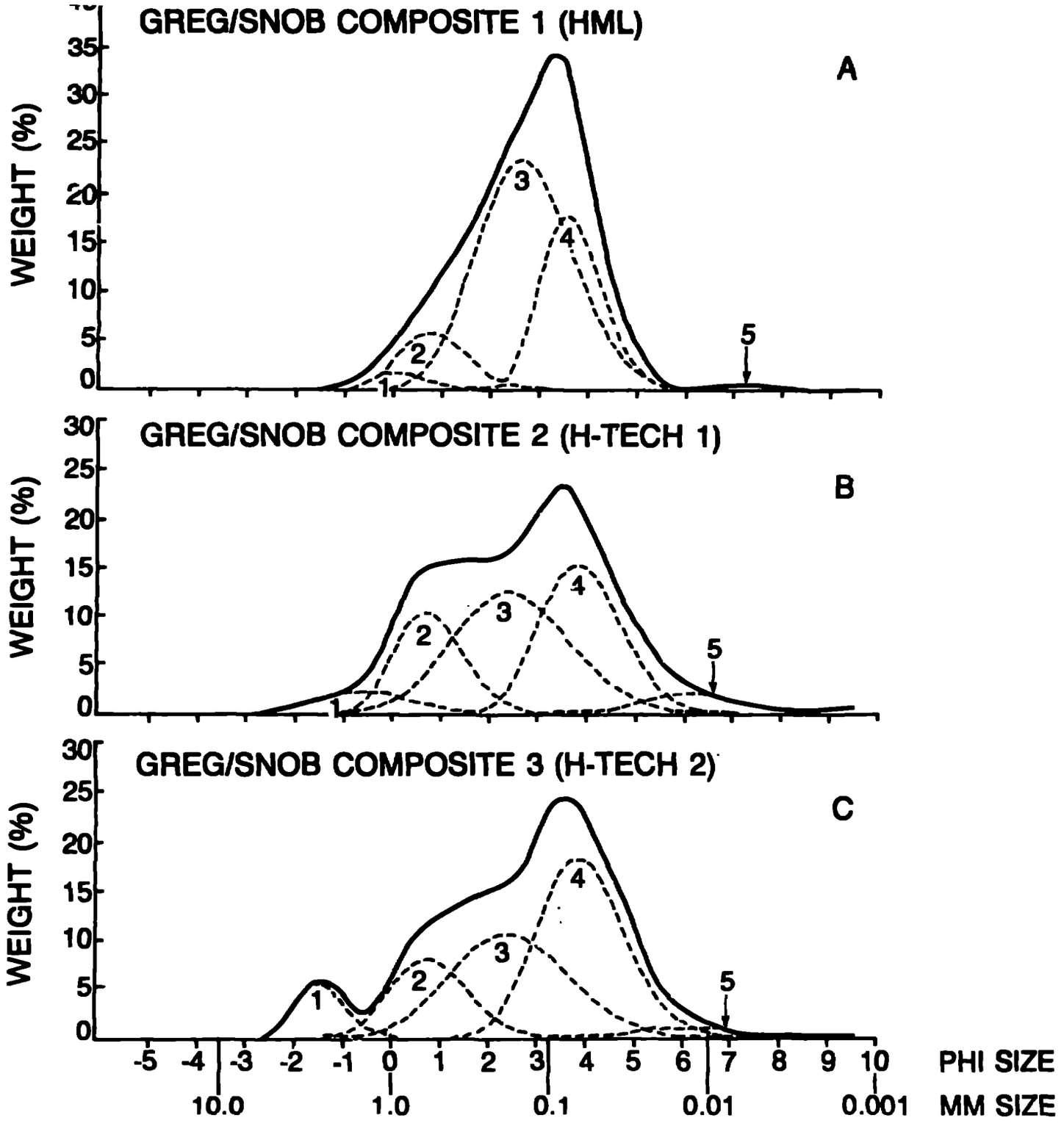
GREG/SNOB COMPOSITE 1 (HML)
A
WEIGHT (%)
35
30
25
20
15
10
5
0
1
2
3
4
5
GREG/SNOB COMPOSITE 2 (H-TECH 1)
B
WEIGHT (%)
30
25
20
15
10
5
0
1
2
3
4
5
GREG/SNOB COMPOSITE 3 (H-TECH 2)
C
WEIGHT (%)
30
25
20
15
10
5
0
1
2
3
4
5
-5 -4 -3 -2 -1 0 1 2 3 4 5 6 7 8 9 10
PHI SIZE
10.0
1.0
0.1
0.01
0.001
MM SIZE

Figure 12